International Journal of Heat and Mass Transfer 52 (2009) 5940–5953

Contents lists available at ScienceDirect

International Journal of Heat and Mass Transfer

journal homepage: www.elsevier.com/locate/ijhmt

Unsteady free convection from elliptic cylinders at large Grashof numbers

S.J.D. D'Alessio *, R.N. Perera

Department of Applied Mathematics, University of Waterloo, Waterloo, Ont., Canada N2L 3G1

ARTICLE INFO

Article history:
Received 10 March 2009
Received in revised form 14 August 2009
Available online 3 September 2009

Keywords:
Viscous
Incompressible
Boussinesq
Elliptic cylinder
Spectral-finite differences
Asymptotic analysis

ABSTRACT

This paper solves the problem of unsteady free convection from an inclined elliptic cylinder both numerically and analytically. An analytical solution valid for small times and large Grashof numbers is derived and compared with numerical solutions to the governing Navier–Stokes and energy equations. The equations are expressed in terms of a streamfunction and vorticity and are solved subject to no-slip and constant heat flux on the surface together with quiescent far-field and initial conditions. Comparisons between the analytical and numerical solutions are made as well as with experiments. Satisfactory agreement is found in all cases.

1. Introduction

Free convective flows initiated impulsively occur naturally in the environment and can be implicated in many industrial applications. Well-documented examples of these flows include impulsively generated free convection from horizontal and vertical flat plates and from two-dimensional cylindrical bodies. Numerous numerical, experimental and theoretical studies devoted to these cases have appeared in the literature over the years. In these studies, some of which include [1–26], free convection is usually a consequence of either a sudden change in surface temperature or a sudden change in surface heat flux.

The focus of the present study is the unsteady problem of laminar, two-dimensional free convective flow from an elliptic cylinder induced by a constant heat flux which is abruptly applied on its surface at $t = 0$. Since this represents a fundamental problem in heat transfer, it is of interest for both theoretical and practical reasons. Some related engineering applications include flow past heated tubes, hot wire anemometry, thermal pollution, and the designing of heat exchangers. The related problems of the heated flat plate and the heated circular cylinder are well studied and some of these works include [1–15].

This problem is addressed analytically and numerically and represents an extension of previous work for small Grashof number flows subject to constant surface temperature [26] to large Grashof number (Gr) flows subject to constant surface heat flux. As pointed out in [24,25], an important feature associated with the elliptic geometry is the increase in the rate of heat transfer.

Closely related existing research on free convection from elliptic cylinders includes the studies of Badr and Shamsher [16] and Mahfouz and Kocabiyik [17] for the symmetrical case and that of Badr [18] for the asymmetrical case. Badr and Shamsher [16] considered elliptic cylinders of various aspect ratios ranging from 0.1 to 0.964 (i.e. approaching a flat plate and circular cylinder, respectively) suspended in air ($Pr = 0.7$). Numerical solutions were performed for Rayleigh numbers ranging from 10 to 1000 for the case of an isothermal surface. Mahfouz and Kocabiyik [17], on the other hand, carried out a numerical study of the transient buoyancy driven flow adjacent to a cylinder of elliptic cross-section with major axis horizontal, whose surface was subjected to a sudden uniform heat flux. This was executed for different values of the modified Rayleigh number ranging from 10^3 to 10^7, Prandtl numbers (Pr) ranging from 0.1 to 10, and cylinder aspect ratios ranging from 0.05 to 0.998.

Some related experimental investigations are those by Huang and Mayinger [19] for elliptic tubes at various inclinations and aspect ratios and by Elsayed, Ibrahim and Elsayed [20] for the case of a constant heat flux from an elliptic tube at large Rayleigh numbers. As for comparisons with experimental studies, the work that is closest to this study is the investigation by Elsayed, Ibrahim and Elsayed [20] which dealt with free convection of air around the outer surface of a horizontal elliptic tube maintained at constant heat flux. In their experiments a stainless steel elliptic tube having a major axis of 90 mm, a minor axis of 50 mm and a length of 1000 mm was used. A cylindrical 1 kW electrical heater having a diameter of 10 mm was placed in the center of the tube and was

* Corresponding author. Tel.: +1 519 888 4567x35014; fax: +1 519 746 0274.
E-mail address: sdalessio@uwaterloo.ca (S.J.D. D'Alessio).

0017-9310/$ - see front matter © 2009 Elsevier Ltd. All rights reserved.
doi:10.1016/j.ijheatmasstransfer.2009.08.008

Nomenclature

b, a	cylinder semi-minor, semi-major axes, respectively
A, B, A_0, B_0, A_1, B_1	functions appearing in governing equations
c	semi-focal length, $c = \sqrt{a^2 - b^2}$
D_1, D_2	functions appearing in the analytical solutions
F_n, f_n	Fourier coefficients for the streamfunction
g	gravitational acceleration
Gr	Grashof number, $Gr = \alpha g c^3 \Delta T/\nu^2$
h_z, h_θ	uniform grid spacing in z, θ directions, respectively
N	number of terms retained in Fourier series
M	metric of transformation
M_0	metric evaluated on the cylinder surface
k	thermal conductivity
$K \times L$	computational grid
p	iteration counter
Pr	Prandtl number, $Pr = \nu/\kappa$
$q, \hat{q}$	functions representing right-hand sides
Q	constant heat flux
r	ellipse aspect ratio, $r = b/a$
r_n, s_n	Fourier coefficients for the vorticity
s	scaled coordinate, $s = M_0 z$
t	time
Δt	time increment in the numerical scheme
T	dimensional temperature
ΔT	temperature scale, $\Delta T = cQ/k$
U	velocity scale, $U = (\alpha c g \Delta T)^{1/2}$
v_ξ, v_θ	velocity components
x, y	Cartesian coordinates
X, Y, f	functions used in separation of variables $\phi_0(w,t) = X(w)Y(t), X(w) = e^{-w^2/2} f(w)$
w	scaled coordinate, $w = \sqrt{Pr} M_0 z$
z	boundary-layer coordinate
z_∞	outer boundary

Greek symbols

α	thermal expansion coefficient
β	computational parameter, $\beta = n\lambda$
ϵ	tolerance
κ	thermal diffusivity
ν	kinematic viscosity
μ	separation constant
ρ	fluid density
ξ, θ	elliptic coordinates
ξ_0	constant related to r, $\tanh \xi_0 = r$
ξ_∞	outer boundary
η	angle of inclination
λ	boundary-layer parameter, $\lambda = \sqrt{4t/\sqrt{Gr}}$
ϕ	dimensionless temperature, $\phi = (T - T_0)/(\Delta T)$
ψ	streamfunction
ζ	vorticity
χ	generic flow variable

Subscripts

0	surface value or leading order terms
∞	value at infinity

Superscript

$\sim$	dimensional quantity
$*$	scaled quantity

used as the heating element. The gap between the heater and the inner surface of the tube was filled with fine sand. The supplied electrical power was measured using a digital watt meter and eight thermocouples were fixed on the tube's surface to measure the local surface temperature. The surface heat flux of the tube was calculated from the electrical power imparted to the heater and the total surface area of the tube. In the experiments the measurements were recorded after 3–4 h of heating when steady-state conditions were achieved. Later we will make comparisons with these experiments by running large-time numerical simulations.

Concerning previous analytical studies, one problem worth mentioning is that of laminar free convection induced by a line source which has been thoroughly reviewed and studied by Liñán and Kurdyumov [27], and by Leal [28]. This refers to a well known analytical solution for steady free convection from a line source of constant heat flux and can be regarded as the asymptotic solution at large distances since from far away the cylinder can be treated as a line source. For large Gr the governing equations can be simplified by making boundary-layer approximations and rescaling the horizontal coordinate and velocity by a factor of $Gr^{1/4}$. An exact similarity solution was found by Yih [29] for Prandtl numbers $Pr = 2, 5/9$. The analytical solution constructed here can be thought of as the opposite extreme case in that the line source solution is valid for large t (i.e. steady state) and at large distances while the solution to be presented in this work is valid for small t and close to the cylinder. It is interesting to point out that both solutions involve the scaling factor of $Gr^{1/4}$.

What distinguishes this study from the others listed above are the following contributions. First, we have formulated an analytical solution procedure for finding an approximate solution to the problem for small time, t, and large Grashof number, Gr. This is accomplished by expanding the flow variables in a double expansion involving two small parameters: t and $\lambda = \sqrt{4t/\sqrt{Gr}}$. As we will see, λ is a parameter that appears naturally in the problem. This extends the analytical solution procedure used in [26] for small Gr (involving a single expansion in t) to large Gr. One of the first studies to adopt a double expansion procedure for an elliptic geometry is that in [30] which was used to study two-dimensional laminar viscous incompressible flows past elliptic cylinders. This work successfully formalizes the procedure for adaption to heat transfer problems. Second, a spectral-finite difference method for numerically integrating the full Navier–Stokes and energy equations is outlined. The method works well in capturing both the small time and large time solutions and works for a wide range of Gr. Third, detailed small-time comparisons between the analytical and numerical solutions are presented, as well as large-time comparisons between experiments and numerical solutions.

The paper is organized as follows. We next present a mathematical formulation of the problem and introduce the governing equations and accompanying boundary and initial conditions along with a convenient coordinate system for the elliptic geometry. In Section 3, we use asymptotic theory to construct an approximate analytical solution which is valid for small times and large Grashof numbers. Section 4 is devoted to outlining a numerical solution procedure to solve the full unsteady Navier–Stokes and energy equations. Following this, in Section 5, we present, discuss and contrast the analytical, numerical and experimental results. Lastly, we include a brief summary of the key points in the concluding section followed by an Appendix A which contains much of the mathematical details related to the asymptotic solution.

2. Mathematical formulation

The equations governing the motion and heat transfer process of a viscous incompressible fluid are the Navier–Stokes and energy equations. The fluid is characterized by the following properties: the kinematic viscosity, ν, the thermal diffusivity, κ, the thermal expansion coefficient, α, and the thermal conductivity, k. While these fluid properties are assumed to remain constant, the fluid density, ρ, is allowed to vary with temperature, T, in the usual fashion

$$\rho(T) = \rho_0[1 - \alpha(T - T_0)],$$

where ρ_0 refers to a reference density and T_0 the corresponding reference temperature. The flow configuration is illustrated in Fig. 1. To render the equations in dimensionless form the chosen length scale is the semi-focal length of the ellipse, $c = \sqrt{a^2 - b^2}$, with a, b denoting the semi-major and semi-minor axis lengths, respectively, the time scale is c/U where U is the velocity scale, soon to be specified, and the temperature scale, ΔT, is related to the surface heat flux, Q, through $\Delta T = cQ/k$. The velocity scale is taken to be $U = (\alpha c g \Delta T)^{1/2}$ where g is the acceleration due to gravity.

Since the flow is assumed to remain two-dimensional it makes sense to work in terms of a streamfunction and vorticity. Also, because of the geometry of the problem it is natural to introduce the modified polar coordinates (ξ, θ) which are related to the Cartesian coordinates (x, y) through the conformal transformation

$$x + iy = \cosh[(\xi + \xi_0) + i\theta].$$

The advantage of this is that the contour of the cylinder is transformed to $\xi = 0$ while the infinite region exterior to the cylinder is mapped to the semi-infinite rectangular strip $0 < \xi < \infty$, $0 \leqslant \theta \leqslant 2\pi$. As shown in Fig. 1, θ is measured in the counterclockwise direction with respect to the positive x axis which corresponds to $\theta = 0$. The constant ξ_0 is defined by

$$\tanh \xi_0 = r,$$

where $r = b/a$ is the ellipse aspect ratio. The above mapping holds for all elliptic cylinders having $0 < r < 1$ with $r = 0$ denoting a flat plate and $r = 1$ a circular cylinder. Another important feature associated with this transformation is that length scales close to the cylinder are unchanged while those far away get contracted. This is helpful from a numerical point of view since the flow field is compressed.

In terms of the coordinates (ξ, θ) the dimensionless laminar unsteady Navier–Stokes and energy equations for a viscous, incompressible fluid in terms of the streamfunction, ψ, vorticity, ζ, and temperature, ϕ, then become

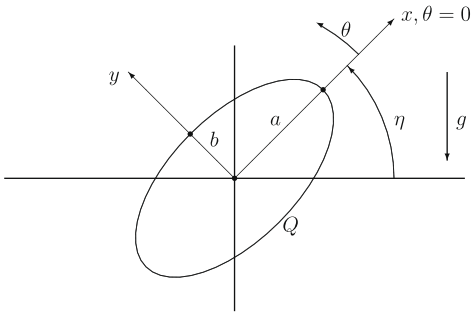

Fig. 1. The flow configuration.

$$\frac{\partial^2\psi}{\partial\xi^2} + \frac{\partial^2\psi}{\partial\theta^2} = M^2\zeta, \tag{1}$$

$$\frac{\partial\zeta}{\partial t} = \frac{1}{M^2}\left[\frac{\partial\psi}{\partial\theta}\frac{\partial\zeta}{\partial\xi} - \frac{\partial\psi}{\partial\xi}\frac{\partial\zeta}{\partial\theta} + \frac{1}{\sqrt{Gr}}\left(\frac{\partial^2\zeta}{\partial\xi^2} + \frac{\partial^2\zeta}{\partial\theta^2}\right) + A\frac{\partial\phi}{\partial\xi} - B\frac{\partial\phi}{\partial\theta}\right], \tag{2}$$

$$\frac{\partial\phi}{\partial t} = \frac{1}{M^2}\left[\frac{\partial\psi}{\partial\theta}\frac{\partial\phi}{\partial\xi} - \frac{\partial\psi}{\partial\xi}\frac{\partial\phi}{\partial\theta} + \frac{1}{\sqrt{Gr}Pr}\left(\frac{\partial^2\phi}{\partial\xi^2} + \frac{\partial^2\phi}{\partial\theta^2}\right)\right], \tag{3}$$

where

$$M^2 = \frac{1}{2}[\cosh(2(\xi + \xi_0)) - \cos(2\theta)],$$
$$A = \sinh(\xi + \xi_0)\cos(\eta)\cos(\theta) - \cosh(\xi + \xi_0)\sin(\eta)\sin(\theta),$$
$$B = \cosh(\xi + \xi_0)\cos(\eta)\sin(\theta) + \sinh(\xi + \xi_0)\sin(\eta)\cos(\theta).$$

The velocity components (v_ξ, v_θ) in the directions of increase of (ξ, θ) are related to the streamfunction through

$$v_\xi = -\frac{1}{M}\frac{\partial\psi}{\partial\theta}, \quad v_\theta = \frac{1}{M}\frac{\partial\psi}{\partial\xi},$$

while the vorticity is found through the expression

$$\zeta = \frac{1}{M^2}\left(\frac{\partial}{\partial\xi}(Mv_\theta) - \frac{\partial}{\partial\theta}(Mv_\xi)\right).$$

The dimensionless parameters appearing in the equations include: the Grashof number, $Gr = \alpha g c^3 \Delta T/\nu^2$, the inclination, η, the Prandtl number, $Pr = \nu/\kappa$, and the ellipse aspect ratio, r. The dimensionless temperature, ϕ, is related to the dimensional temperature, T, through $\phi = (T - T_0)/\Delta T$ where T_0 is taken to be the constant far-field temperature. Similarly, $\psi = \tilde{\psi}/(cU)$ and $\zeta = c\tilde{\zeta}/U$ with the tilde denoting a dimensional quantity. Lastly, in arriving at the above equations we have made the Boussinesq approximation to account for buoyancy and have omitted viscous dissipation.

We assume that at $t = 0$ an impulsive heat flux is applied to the cylinder surface and that both the cylinder surface and surrounding fluid have an initial temperature of T_0. Eqs. (1)–(3) are to be solved subject to the no-slip and constant heat flux conditions on the surface given by

$$\psi = \frac{\partial\psi}{\partial\xi} = 0 \quad \text{and} \quad \frac{1}{M}\frac{\partial\phi}{\partial\xi} = -1 \quad \text{on } \xi = 0. \tag{4}$$

Inspecting these conditions we observe that two conditions for the streamfunction are given while none for the vorticity is provided. Later we will discuss a method to prescribe the surface vorticity. Dennis and Quartapelle [31] have shown that the vorticity field satisfies integral constraints. These conditions can be derived from the no-slip boundary conditions using Green's second identity and are given by

$$\int_0^\infty \int_0^{2\pi} e^{-n\xi} M^2\zeta \sin(n\theta) d\theta d\xi = 0, \quad n = 1, 2, \ldots,$$
$$\int_0^\infty \int_0^{2\pi} e^{-n\xi} M^2\zeta \cos(n\theta) d\theta d\xi = 0, \quad n = 0, 1, \ldots \tag{5}$$

At large distances we impose

$$\psi, \zeta, \phi \to 0 \quad \text{as } \xi \to \infty, \tag{6}$$

which correspond to a quiescent far-field flow maintained at a constant temperature. Lastly, we need to specify initial conditions. Since the fluid initially has a uniform temperature and the motion starts from rest, the initial conditions are simply

$$\psi(\xi, \theta, t = 0) = \zeta(\xi, \theta, t = 0) = \phi(\xi, \theta, t = 0) = 0. \tag{7}$$

To better resolve the early stages of the flow and heat transfer process following the impulsive startup at $t = 0$, the boundary-layer coordinate, z, defined by

$$z = \frac{\xi}{\lambda} \quad \text{where } \lambda = \sqrt{\frac{4t}{\sqrt{Gr}}}, \tag{8}$$

is introduced. Essentially, this change of variable stretches the thermal-boundary layer with λ describing the diffusive growth of the evolving boundary layer. Another advantage of working in terms of the coordinate z is that the physical coordinate ξ becomes a moving coordinate; that is, lines of constant z expand in time when plotted in a Cartesian coordinate system. This is ideal from a numerical point of view, since the grid lines are alive and allowed to expand with the growing boundary layer to ensure adequate resolution during the early stages. In terms of the coordinate z, Eqs. (1)–(3) get transformed to

$$\frac{\partial^2\psi}{\partial z^2} + \lambda^2\frac{\partial^2\psi}{\partial\theta^2} = \lambda^2 M^2\zeta, \tag{9}$$

$$\frac{1}{M^2}\frac{\partial^2\zeta}{\partial z^2} + 2z\frac{\partial\zeta}{\partial z} = 4t\frac{\partial\zeta}{\partial t} - \frac{\lambda^2}{M^2}\frac{\partial^2\zeta}{\partial\theta^2} + \frac{4t}{\lambda M^2}\left(\frac{\partial\psi}{\partial z}\frac{\partial\zeta}{\partial\theta} - \frac{\partial\psi}{\partial\theta}\frac{\partial\zeta}{\partial z}\right) - \frac{4tA}{\lambda M^2}\frac{\partial\phi}{\partial z} + \frac{4tB}{M^2}\frac{\partial\phi}{\partial\theta}, \tag{10}$$

$$\frac{1}{PrM^2}\frac{\partial^2\phi}{\partial z^2} + 2z\frac{\partial\phi}{\partial z} = 4t\frac{\partial\phi}{\partial t} - \frac{\lambda^2}{PrM^2}\frac{\partial^2\phi}{\partial\theta^2} + \frac{4t}{\lambda M^2}\left(\frac{\partial\psi}{\partial z}\frac{\partial\phi}{\partial\theta} - \frac{\partial\psi}{\partial\theta}\frac{\partial\phi}{\partial z}\right), \tag{11}$$

while conditions (4)–(7) become

$$\psi = \frac{\partial\psi}{\partial z} = 0 \quad \text{and} \quad \frac{1}{M}\frac{\partial\phi}{\partial z} = -\lambda \quad \text{on } z = 0, \tag{12}$$

$$\int_0^\infty\int_0^{2\pi} e^{-n\lambda z}M^2\zeta\sin(n\theta)d\theta dz = 0, \quad n = 1,2,\ldots,$$
$$\int_0^\infty\int_0^{2\pi} e^{-n\lambda z}M^2\zeta\cos(n\theta)d\theta dz = 0, \quad n = 0,1,\ldots, \tag{13}$$

$$\psi,\zeta,\phi \to 0 \quad \text{as } z\to\infty, \tag{14}$$

$$\psi(z,\theta,t=0) = \zeta(z,\theta,t=0) = \phi(z,\theta,t=0) = 0. \tag{15}$$

As a final note we emphasize that although the boundary-layer coordinate z is utilized, the fully nonlinear Navier–Stokes and energy equations are to be solved and not the simplified thermal-boundary layer equations. We next outline how to construct an approximate analytical solution to the system of Eqs. (9)–(11).

3. Analytical solution procedure

While there are several analytical techniques available for deriving an approximate solution for the early development of the flow and heat transfer process, the approach adopted here is the multiple series expansion method. The key advantage offered by this method is that it provides a systematic procedure which reduces the problem to a set of linear ordinary differential equations having a specific form. In addition, a multiple series expansion is actually suggested by the physics of the problem. This can be seen by examining Eqs. (1)–(3) and making the usual boundary-layer type approximations which leads to the simplified set of equations for the leading order terms $\hat{\psi}, \hat{\zeta}$ and $\hat{\phi}$

$$\frac{\partial^2\hat{\psi}}{\partial\xi^2} = M_0^2\hat{\zeta}, \tag{16}$$

$$\frac{\partial\hat{\zeta}}{\partial t} = \frac{1}{M_0^2}\left(\frac{1}{\sqrt{Gr}}\frac{\partial^2\hat{\zeta}}{\partial\xi^2} + A_0\frac{\partial\hat{\phi}}{\partial\xi}\right), \tag{17}$$

$$\frac{\partial\hat{\phi}}{\partial t} = \frac{1}{M_0^2 Pr\sqrt{Gr}}\frac{\partial^2\hat{\phi}}{\partial\xi^2}, \tag{18}$$

where $M_0^2(\theta) = M^2(\xi = 0,\theta)$ and $A_0(\theta) = A(\xi = 0,\theta)$.

Eqs. (16)–(18) can be thought of as the conduction equations since they exploit the fact that for very small times the fluid can be taken to be at rest and conduction in the radial direction is the heat transfer mechanism responsible for establishing a temperature gradient which in turn induces motion through the resulting buoyancy force. The solution to this system of coupled linear partial differential equations can be found by first solving the energy Eq. (18). The solution satisfying the boundary conditions (4) and (6) is found to be

$$\hat{\phi}(\xi,\theta,t) = \sqrt{\frac{4t}{\sqrt{Gr}}}\left[\frac{1}{\sqrt{\pi Pr}}\exp\left(-\frac{M_0^2 Pr\xi^2}{\frac{4t}{\sqrt{Gr}}}\right) - \frac{M_0\xi}{\sqrt{\frac{4t}{\sqrt{Gr}}}}\operatorname{erfc}\left(\frac{\sqrt{Pr}M_0\xi}{\sqrt{\frac{4t}{\sqrt{Gr}}}}\right)\right], \tag{19}$$

where

$$\operatorname{erf}(x) = \frac{2}{\sqrt{\pi}}\int_0^x e^{-u^2}du,$$

is the error function and $\operatorname{erfc}(x) = 1 - \operatorname{erf}(x)$ is the complimentary error function. Expressed this way we see that the solution naturally involves the similarity variable $z = \xi/\lambda$ and the parameter $\lambda = \sqrt{4t/\sqrt{Gr}}$. This supports using Eqs. (9)–(11) to dictate the early stages of the problem. The solutions for $\hat{\psi}$ and $\hat{\zeta}$ can then be obtained by substituting (19) into (17), although these details will not be presented. As shown in Appendix A, the solution given by Eq. (19) represents the first non-zero term in the expansion for the temperature.

We now formally discuss the multiple series expansion method. The procedure involves expanding the flow variables in powers of the parameter λ which will be small if t is small or if Gr is large. It turns out that if this is done the resulting equations are still too complicated to solve analytically. If t is taken to be small and Gr is taken to be large then we can identify two small parameters appearing in the problem, λ and t, and it is then possible to expand the flow variables in a double series as follows. First, we expand ϕ,ζ and ψ in a series of the form

$$\phi = \phi_0 + \lambda\phi_1 + \lambda^2\phi_2 + \cdots,$$
$$\zeta = \zeta_0 + \lambda\zeta_1 + \lambda^2\zeta_2 + \cdots,$$
$$\psi = \psi_0 + \lambda\psi_1 + \lambda^2\psi_2 + \cdots.$$

Then each $\phi_n,\zeta_n,\psi_n, n = 0,1,2,\ldots,$ are further expanded in a series of the form

$$\phi_n(z,\theta,t) = \phi_{n0}(z,\theta) + t\phi_{n1}(z,\theta) + \cdots,$$
$$\zeta_n(z,\theta,t) = \zeta_{n0}(z,\theta) + t\zeta_{n1}(z,\theta) + \cdots,$$
$$\psi_n(z,\theta,t) = \psi_{n0}(z,\theta) + t\psi_{n1}(z,\theta) + \cdots.$$

We note that when performing a double expansion the internal orders of magnitudes between the expansion parameters should be taken into account. In our case, λ and t will be equal when $t = 4/\sqrt{Gr}$, and thus, for a fixed value of Gr the procedure is expected to be valid for times that are of order $1/\sqrt{Gr}$ provided that Gr is sufficiently large. Fortunately, asymptotic expansions are known to have the redeeming feature that they often provide good

results outside the domain of validity. This will be discussed in more detail when we make comparisons with numerical solutions.

Since the governing equations also involve the functions M^2, A and B, it will be necessary to expand these functions as well. Doing this yields:

$$M^2 = M_0^2(\theta) + \sinh(2\xi_0)\lambda z + \cosh(2\xi_0)\lambda^2 z^2 + \cdots,$$
$$A(z,\theta) = A_0(\theta) + A_1(\theta)\lambda z + \frac{A_0(\theta)}{2}\lambda^2 z^2 + \cdots,$$
$$B(z,\theta) = B_0(\theta) + B_1(\theta)\lambda z + \frac{B_0(\theta)}{2}\lambda^2 z^2 + \cdots,$$

where

$$M_0^2 = \frac{1}{2}[\cosh(2\xi_0) - \cos(2\theta)],$$
$$A_0(\theta) = \sinh(\xi_0)\cos(\eta)\cos(\theta) - \cosh(\xi_0)\sin(\eta)\sin(\theta),$$
$$A_1(\theta) = \cosh(\xi_0)\cos(\eta)\cos(\theta) - \sinh(\xi_0)\sin(\eta)\sin(\theta),$$
$$B_0(\theta) = \cosh(\xi_0)\cos(\eta)\sin(\theta) + \sinh(\xi_0)\sin(\eta)\cos(\theta),$$
$$B_1(\theta) = \sinh(\xi_0)\cos(\eta)\sin(\theta) + \cosh(\xi_0)\sin(\eta)\cos(\theta).$$

Substituting the above series into Eqs. (9)–(11) produces a hierarchy of problems at various orders. At each order the solution strategy is similar to that in solving Eqs. (16)–(18); that is, we first solve for the temperature and then use it to obtain the vorticity and finally we solve for the streamfunction using the determined vorticity.

Applying this procedure we have derived the following approximate solutions:

$$\phi = \lambda\phi_{10} + \lambda^2\phi_{20} + O(\lambda^2 t^2 + \lambda^3),$$
$$\zeta = t\zeta_{01} + O(t^2 + \lambda t),$$
$$\psi = \lambda^2 t\psi_{21} + O(\lambda^3).$$

The expressions for the various terms listed along with the mathematical details can be found in Appendix A. Before comparing the above constructed approximate analytical solutions with fully numerical solutions, we first present the numerical solution procedure in the following section.

4. Numerical solution procedure

As previously mentioned the early stages of the flow are to be computed using Eqs. (9)–(11) involving the boundary-layer coordinate z. Once the boundary layer thickens appreciably one can switch back to the original coordinate ξ and solve Eqs. (1)–(3). A convenient time to make the switch is when $t = \sqrt{Gr}/4$ since at this time $\lambda = 1$ and hence $\xi = z$. However, for large Gr it is more practical to work entirely in the boundary-layer coordinate z. We will first outline the procedure for solving Eqs. (9)–(11) since these are the equations dictating the initial stages.

We begin by discretizing the computational domain bounded by $0 \leqslant z \leqslant z_\infty$ and $0 \leqslant \theta \leqslant 2\pi$ into a uniform network of $K \times L$ grid points located at

$$z_i = ih_z, \quad i = 0, 1, \ldots, K, \quad \text{where } h_z = \frac{z_\infty}{K},$$
$$\text{and } \theta_j = jh_\theta, \quad j = 0, 1, \ldots, L, \text{ where } h_\theta = \frac{2\pi}{L},$$

with z_∞ denoting the outer boundary approximating infinity.

The streamfunction is solved by expanding it into the truncated Fourier series

$$\psi(z,\theta,t) = \frac{1}{2}F_0(z,t) + \sum_{n=1}^{N}[F_n(z,t)\cos(n\theta) + f_n(z,t)\sin(n\theta)],$$

where the Fourier coefficients satisfy

$$\frac{\partial^2 F_n}{\partial z^2} - n^2\lambda^2 F_n = \lambda^2 s_n(z,t), \quad n = 0, 1, \ldots, \tag{20}$$
$$\frac{\partial^2 f_n}{\partial z^2} - n^2\lambda^2 f_n = \lambda^2 r_n(z,t), \quad n = 1, \ldots, \tag{21}$$

with

$$s_n(z,t) = \frac{1}{\pi}\int_0^{2\pi} M^2\zeta\cos(n\theta)d\theta \text{ and } r_n(z,t) = \frac{1}{\pi}\int_0^{2\pi} M^2\zeta\sin(n\theta)d\theta.$$

Boundary conditions for the Fourier components can easily be determined from those for the streamfunction. Further conditions satisfied by the functions $r_n(z,t)$ and $s_n(z,t)$ follow from the integral conditions and are given by

$$\int_0^\infty e^{-n\lambda z}s_n(z,t)dz = 0, \quad n = 0, 1, 2, \ldots$$
$$\text{and} \qquad \int_0^\infty e^{-n\lambda z}r_n(z,t)dz = 0, \quad n = 1, 2, \ldots$$

The above play an important role in determining the surface vorticity as we shall shortly see.

Eqs. (20) and (21) at a fixed time are of the form

$$h''(z) - \beta^2 h(z) = g(z),$$

where $\beta = n\lambda$ and the prime refers to differentiation with respect to z. These ordinary differential equations can be integrated using step-by-step formulae. The important point to note here is that the particular marching algorithm to be used is dependent on the parameter β. Two sets of step-by-step methods were utilized: one for $\beta < 0.5$ while another one for $\beta \geqslant 0.5$. The specific schemes used can be found in [30].

To discuss the numerical method used to solve Eqs. (10) and (11) we begin by rewriting them in the generic form

$$t\frac{\partial\chi}{\partial t} = q(z,\theta,t).$$

The scheme used to discretize this equation is very similar to the Crank–Nicholson implicit procedure. Assuming the solution at time t is known, we advance the solution to time $t + \Delta t$ by integrating the above. Integration by parts yields

$$\chi\tau|_t^{t+\Delta t} - \int_t^{t+\Delta t}\chi d\tau = \int_t^{t+\Delta t} q d\tau,$$

where Δt is the time increment. Approximating the integrals using the trapezoidal rule results in the expression

$$\chi(z,\theta,t+\Delta t) = \chi(z,\theta,t) + \left(\frac{\Delta t}{2t+\Delta t}\right)[q(z,\theta,t+\Delta t) + q(z,\theta,t)].$$

Since $q(z,\theta,t+\Delta t)$ depends on $\chi(z,\theta,t+\Delta t)$ and its spatial derivatives the scheme is implicit. This equation is solved iteratively using a Gauss–Seidel procedure. All spatial derivatives appearing in the function q are approximated using central-differences; thus the scheme given is second order accurate in both space and time.

The boundary conditions used in solving the energy equation are straight-forward and require no explanation. For the vorticity transport equation, on the other hand, careful attention must be given to determine the surface vorticity. The surface vorticity can be determined by inverting the expressions for r_n and s_n and leads to the truncated Fourier series

$$\zeta(0,\theta,t) = \frac{1}{M_0^2}\left\{\frac{1}{2}s_0(0,t) + \sum_{n=1}^{N}[r_n(0,t)\sin(n\theta) + s_n(0,t)\cos(n\theta)]\right\},$$

where $M_0^2 = M^2(z=0,\theta)$. The quantities $s_n(0,t)$ and $r_n(0,t)$ are computed by enforcing the integral conditions; that is, off the cylinder surface r_n and s_n can be computed using the most recent guess for

ζ. Then, $s_n(0,t)$ and $r_n(0,t)$ are computed by numerically satisfying the integral constraints.

The numerical method used for solving Eqs. (1)–(3) is very similar to the procedure described above. We will focus on the solution of Eqs. (2) and (3) since the method used to solve Eq. (1) is identical to that used in solving (9). The only difference worth pointing out is that for $t > \sqrt{Gr}/4$ Eqs. (2) and (3) can be rewritten in the generic form

$$\frac{\partial \chi}{\partial t} = \hat{q}(\xi, \theta, t).$$

Using the same differencing strategy as previously outlined we arrive at the following scheme for solving the above transport equation

$$\chi(\xi, \theta, t + \Delta t) = \chi(\xi, \theta, t) + \frac{\Delta t}{2}[\hat{q}(\xi, \theta, t + \Delta t) + \hat{q}(\xi, \theta, t)].$$

We summarize the numerical method by listing the steps involved in the procedure. Assuming all quantities are known at time t and wish to advance the solution to time $t + \Delta t$, we perform the following steps (p denotes the iteration counter):

1. Solve for $\phi^{(p)}(z, \theta, t + \Delta t)$,
2. Solve for $\zeta^{(p)}(z, \theta, t + \Delta t)$ everywhere except on the cylinder surface ($z = 0$),
3. Compute $r_n^{(p)}(z, t + \Delta t)$, $s_n^{(p)}(z, t + \Delta t)$ for $z \neq 0$,
4. Calculate $r_n^{(p)}(0, t + \Delta t)$, $s_n^{(p)}(0, t + \Delta t)$ by enforcing the integral conditions and hence compute $\zeta^{(p)}(0, \theta, t + \Delta t)$,
5. Solve for $f_n^{(p)}(z, t + \Delta t)$, $F_n^{(p)}(z, t + \Delta t)$ and thus obtain $\psi^{(p)}(z, \theta, t + \Delta t)$, and
6. Repeat above steps till convergence is reached and increment p by 1 after each complete iteration.

Step (4) indicates how the integral conditions are used in determining the surface vorticity. It may also be necessary to subject the surface vorticity to under-relaxation in order to obtain convergence. Convergence is reached when the difference between two successive iterates of the surface vorticity falls below some specified tolerance ϵ.

Numerical results together with comparisons with the analytical solution and experimental data will next be presented.

5. Results, comparisons and discussion

The problem of free convection from an inclined elliptic cylinder is completely characterized by the parameters Gr, Pr, η and r. After performing numerous numerical experiments, the following computational parameters were chosen: $N = 25, \epsilon = 10^{-6}$, $z_\infty = 10$. A typical grid size used was $K \times L = 200 \times 120$. Because of the impulsive start, very small time steps of $\Delta t = 10^{-4}$ were used initially to get past the singularity at $t = 0$. As time increased the time step was gradually increased to $\Delta t = 0.05$. Results were obtained for parameter values in the following ranges: $r = 0.2$—$0.8, \eta = 0$—90° and $Gr = 10^2$—10^7. For most of the simulations the Prandtl number was fixed at $Pr = 0.7$ which corresponds to air.

We begin by making comparisons between the analytical and numerical results which will focus on the surface temperature and vorticity. The time variation of the average surface temperature for the case $Gr = 10^6, r = 0.5$ and $\eta = 45^\circ$ is contrasted in Fig. 2. It is interesting to point out that for $Gr = 10^6$ the analytical solution is expected to be valid for times up to about $t \sim 4/\sqrt{Gr} = 0.004$. However, as the plot reveals the agreement is good for much larger times and it worsens as time increases, which is to be expected.

We next compare the surface temperature distribution at various times for the case $Gr = 10^4, r = 0.5$ and $\eta = 45^\circ$ in Fig. 3. It is clear that the agreement is better over the flatter sections than near the tips of the ellipse, located at $\theta = 0$ and $\theta = 180^\circ$. We also observe that the temperature profiles are symmetric with temperature drops occurring near the tips due to curvature effects. Since a constant heat flux is applied on the cylinder surface, the energy transferred to each section is the same and thus the temperature decreases more over sections having larger curvature than those having smaller curvature. The agreement in the surface temperature distribution is not as good as that with the average surface temperature. The averaging process has the effect of hiding the larger errors occurring at the tips. Fig. 3 also illustrates how the agreement persists for times outside the expected region of

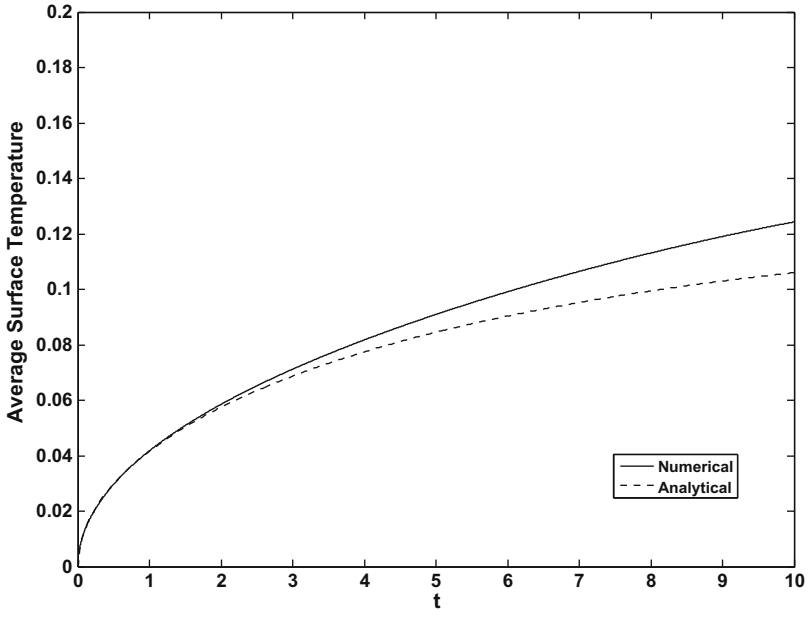

Fig. 2. The time variation of the average surface temperature for the case $Gr = 10^6, Pr = 0.7, r = 0.5$ and $\eta = 45^\circ$.

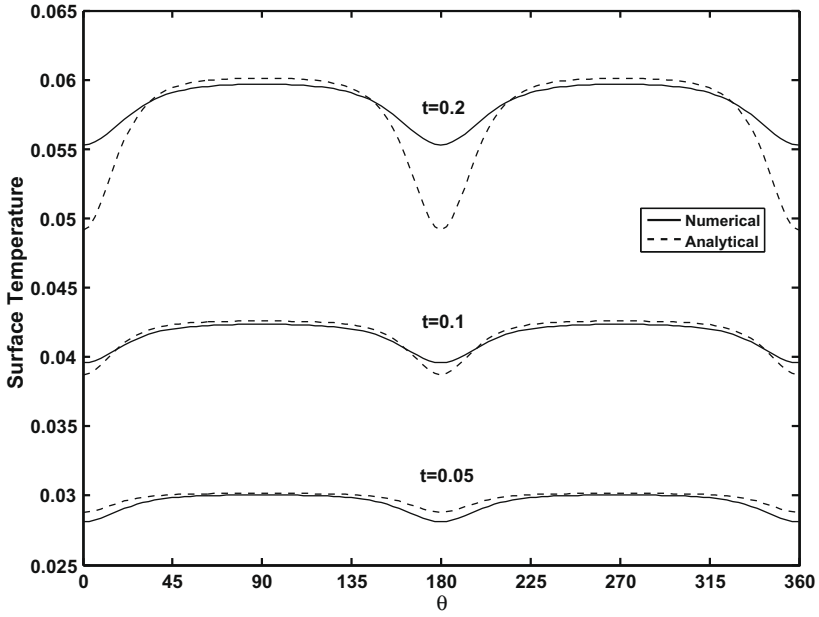

Fig. 3. Surface temperature distributions for the case $Gr = 10^4, Pr = 0.7, r = 0.5$ and $\eta = 45^\circ$ at times $t = 0.05, 0.1, 0.2$.

validity $0 < t < 4/\sqrt{Gr}$. For larger Gr this agreement persists for even larger times as shown in Fig. 4.

Shown in Fig. 5 are the surface vorticity distributions at times $t = 0.05$ and 0.1 for the case $Gr = 10^4, r = 0.5$ and $\eta = 45^\circ$. The agreement between the numerical and analytical solutions is not as good for the vorticity because fewer terms were retained in that series. In fact, the agreement does not change much even if Gr is increased to $Gr = 10^6$ because the leading-order, and hence dominant, term in the vorticity expansion does not depend on Gr. The surface vorticity distributions, which resemble negative sine curves, become zero at $\theta \approx 25^\circ$ and $\theta \approx 200^\circ$ and is positive (or rotates counterclockwise) in the ranges $0 \leqslant \theta \lesssim 25^\circ$ and $200^\circ \lesssim \theta \lesssim 360^\circ$ and negative (or rotates clockwise) between $25^\circ \lesssim \theta \lesssim 200^\circ$. This makes physical sense since the directions of rotation suggest the paths that buoyant fluid elements near the surface will follow before ultimately rising vertically. It is worth making some connections between the results obtained here and those reported in [32] for the case of a cylinder having a constant surface temperature at small Grashof numbers for small times. Both problems involve an abrupt startup resulting from an initial discontinuity. In [32] the initial discontinuity is in temperature while here it is in the heat flux. The difference in the nature of these discontinuities arise from the different boundary conditions applied. Both discontinuities, however, lead to the same result which is to heat the fluid adjacent to the surface by conduction thus causing the heated fluid to rise. While quantitative comparisons in surface vorticity distributions cannot be made, qualitative comparisons can be drawn. Apart from a scaling, the surface

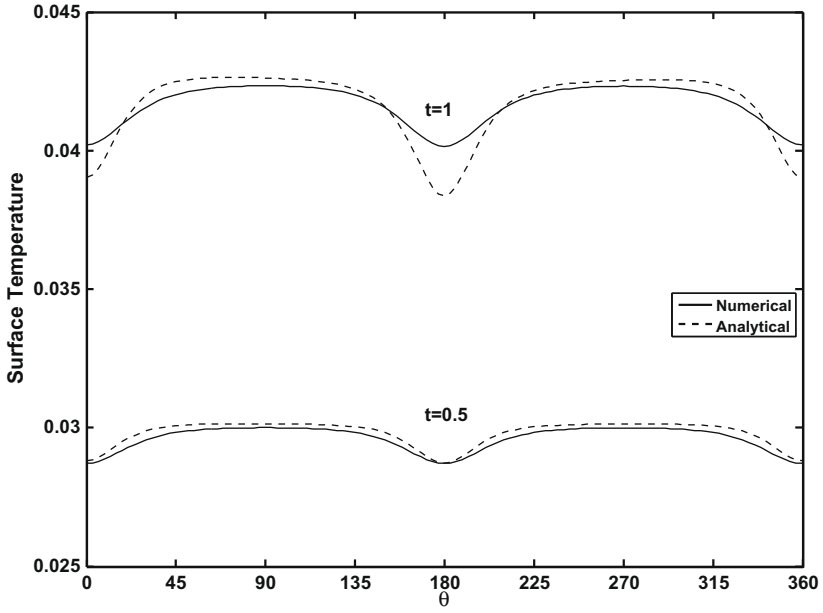

Fig. 4. Surface temperature distributions for the case $Gr = 10^6, Pr = 0.7, r = 0.5$ and $\eta = 45^\circ$ at times $t = 0.5, 1$.

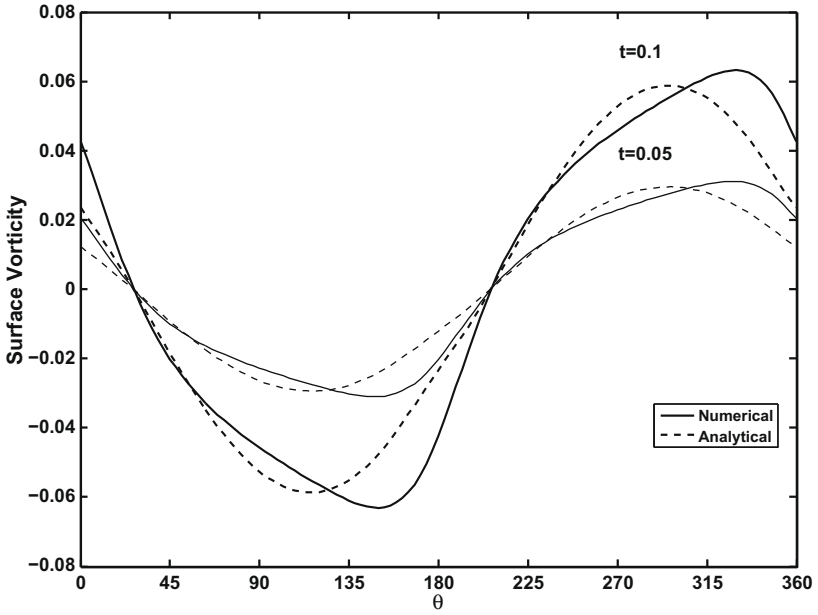

Fig. 5. Surface vorticity distributions for the case $Gr = 10^4, Pr = 0.7, r = 0.5$ and $\eta = 45^\circ$ at times $t = 0.05, 0.1$.

vorticity distributions obtained here are very similar to those obtained in [32]. This is quite interesting given that the equations used in the two studies are significantly different due to the different scalings adopted. The difference in the scaling of the vorticity distributions is a result of the different ranges in Grashof numbers considered; [32] focused on small *Gr* while this study focuses on large *Gr*.

The level of agreement will also depend on the parameters *r* and η. We expect the agreement to improve as *r* increases (approaching a circular geometry), and when $\eta = 0^\circ$ or 90° (i.e. minor or major axis is aligned with gravity, respectively). Fig. 6, confirms this prediction for the case $\eta = 90^\circ$ and $r = 0.8$. Similar agreement was found when $\eta = 0$. Notice that the temperature distribution is almost uniform as one would expect to get for a circular cylinder since it has constant curvature. On the other hand, we expect the agreement to worsen when *r* decreases and when $\eta \neq 0, 90^\circ$ (i.e. the cylinder configuration is not aligned with gravity). This is also confirmed in Fig. 7 for the case $r = 0.3$ and $\eta = 45^\circ$. Note that the temperature distribution gets flatter as *r* decreases with larger temperature changes near the tips. Recall that the mapping used is valid for $0 < r < 1$. We have observed that the analytical solution gives physical results for the range $0.25 \lesssim r \lesssim 0.85$. Outside this interval the analytical solution breaks down; that is, there is a temperature increment near the tips instead of a decrement.

Having established the small-time behavior, we next discuss isotherm plots obtained by our numerical simulations for moderate to large times. Shown in Figs. 8 and 9 are isotherm plots at times $t = 2.5, 100$, respectively, for the case $Gr = 10^2, r = 0.5$ and $\eta = 45^\circ$. In all isotherm plots to be presented the outermost contour corresponds to $\phi = 0.05$ and the spacing between consecutive

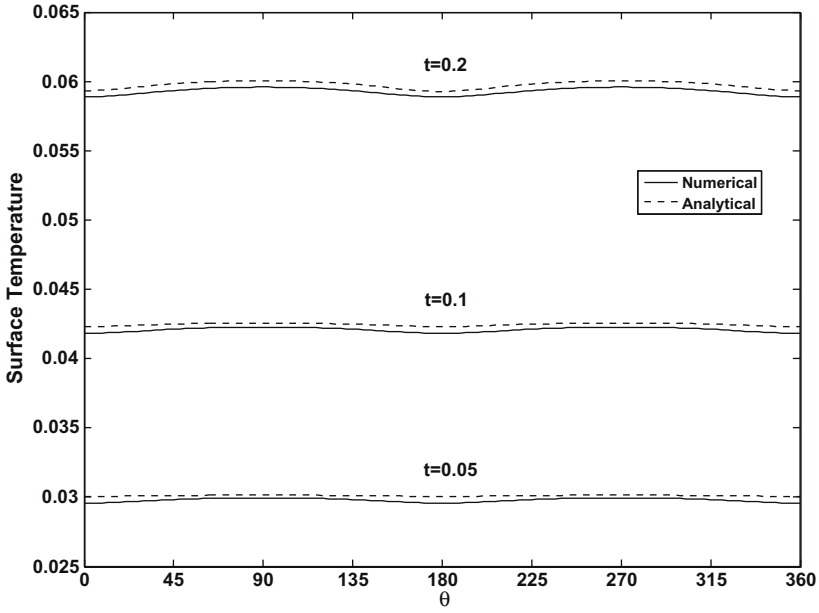

Fig. 6. Surface temperature distributions for the case $Gr = 10^4, Pr = 0.7, r = 0.8$ and $\eta = 90^\circ$ at times $t = 0.05, 0.1, 0.2$.

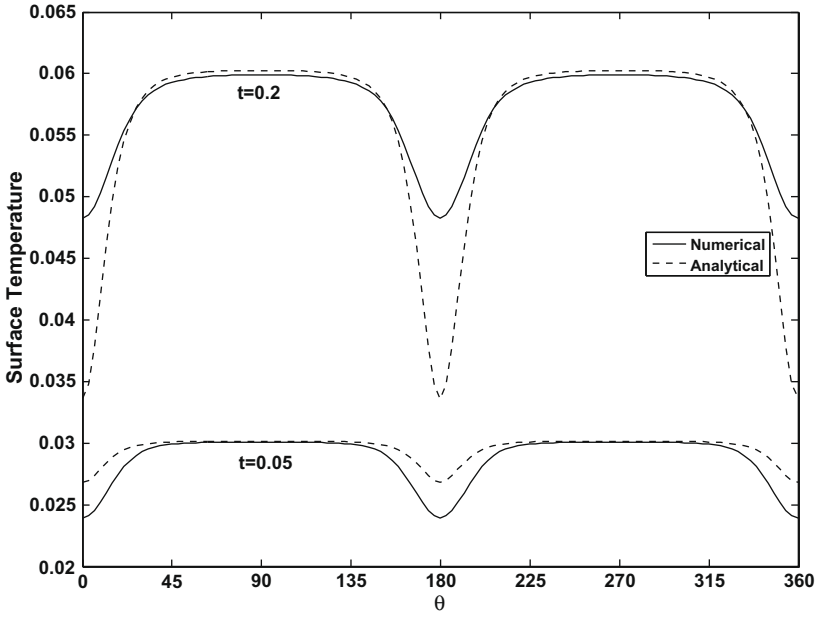

Fig. 7. Surface temperature distributions for the case $Gr = 10^4, Pr = 0.7, r = 0.3$ and $\eta = 45^\circ$ at times $t = 0.05, 0.2$.

contours is $\Delta\phi = 0.05$. For this case Eqs. (9)–(11) in the boundary-layer coordinate z were integrated up to $t = 2.5$ (i.e. $\lambda = 1$) after which Eqs. (1)–(3) and were solved. The isotherms portrayed in Fig. 8 appear to form concentric rings. For small to moderate times this is to be expected as this corresponds to the conduction regime. For large times, as depicted in Fig. 9, a well developed thermal plume forms. In Fig. 10 the Grashof number is increased to $Gr = 10^4$. For this larger Grashof number computations were carried out entirely in the boundary-layer coordinate. Witnessed in the isotherm plot displayed in Fig. 10 at $t = 20$ is the formation of a well defined plume. For large Gr the plume develops much sooner due to the enhanced buoyancy force. Lastly, surface temperature and vorticity distributions are plotted in Figs. 11 and 12, respectively, at various times again for $Gr = 10^4$. As time advances both distributions seem to be approaching a steady profile and reveal a prominent maximum evolving in the vicinity of one of the tips of the cylinder.

Our simulations suggest that the average surface temperature appears to approach a steady-state value, $\overline{\phi}_s$, as time advances. This provides an opportunity to make connections with the steady-state experiments performed by Elsayed, Ibrahim and Elsayed [20]. The parameters used in their experiments are: $Pr = 0.7, r = 0.556$ and $\eta = 90^\circ$. The Grashof number varied according to the heat flux prescribed and are listed in Table 1. From their five discrete data points for the surface temperature (i.e. $(T_s - T_0)$ in Fig. 2 of Ref. [20]) $\overline{\phi}_s$ was estimated using

$$\overline{\phi}_s \approx \frac{1}{5\Delta T}\sum_{i=1}^{5}(T_s - T_0)_i, \quad \text{where } \Delta T = \frac{cQ}{k}.$$

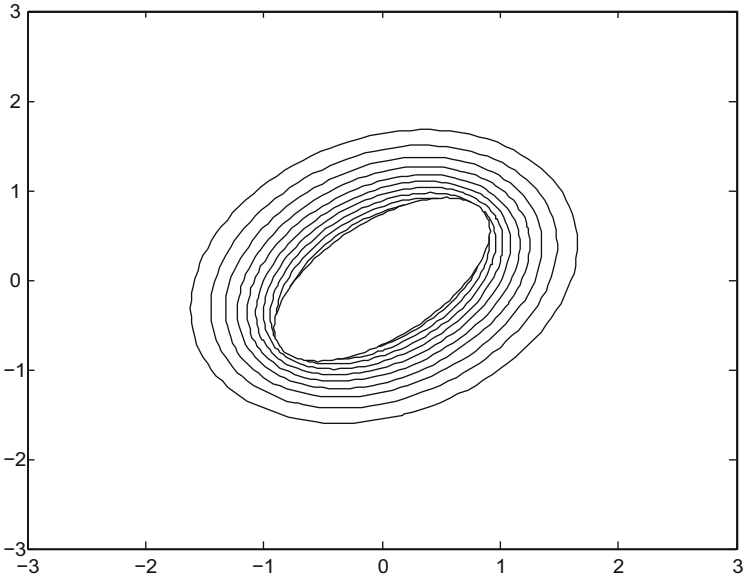

Fig. 8. Isotherm plot at $t = 2.5$ for the case $Gr = 10^2, Pr = 0.7, r = 0.5$ and $\eta = 45^\circ$.

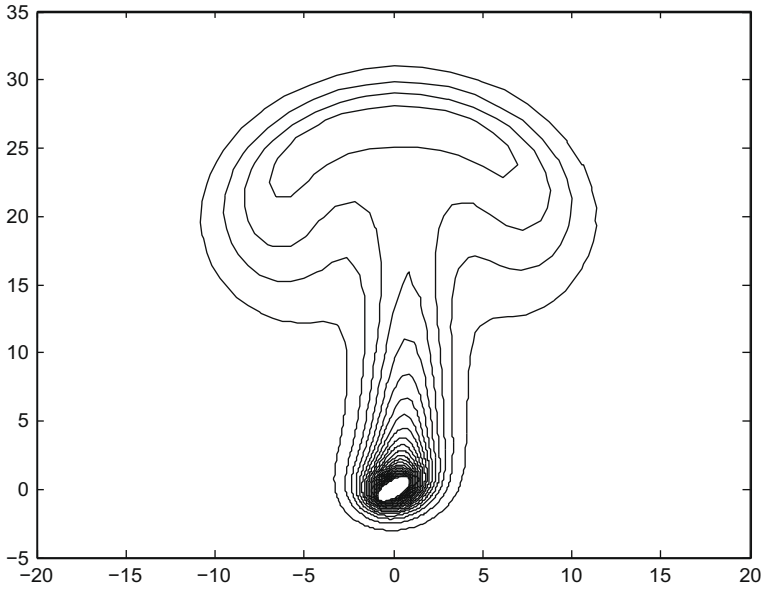

Fig. 9. Isotherm plot at $t = 100$ for the case $Gr = 10^2, Pr = 0.7, r = 0.5$ and $\eta = 45^\circ$.

Table 1 compares the experimental values of $\overline{\phi}_s$ with our corresponding computed values for the heat fluxes applied in their experiments. We see that the agreement worsens as the heat flux increases. This should come as no surprise since our laminar Boussinesq fluid model will eventually breakdown when the flow becomes turbulent. Also, as the heat flux increases so will the resulting temperature difference between the surface and ambient surroundings, $(T_s - T_0)$, and our linear equation of state will no longer be realistic.

The dependence of $\overline{\phi}_s$ on the parameters Gr and Pr for the limiting cases $Gr \gg 1, Pr \gg 1$ and $Gr \gg 1, Pr \ll 1$ can be established from scaling arguments as follows. In the thermal-boundary layer the dominant terms in the steady-state versions of Eqs. (1)–(3) are

$$\frac{\partial^2 \psi}{\partial \xi^2} = M_0^2 \zeta, \tag{22}$$

$$\frac{\partial \psi}{\partial \theta}\frac{\partial \zeta}{\partial \xi} - \frac{\partial \psi}{\partial \xi}\frac{\partial \zeta}{\partial \theta} + \frac{1}{\sqrt{Gr}}\frac{\partial^2 \zeta}{\partial \xi^2} + A_0 \frac{\partial \phi}{\partial \xi} = 0, \tag{23}$$

$$\frac{\partial \psi}{\partial \theta}\frac{\partial \phi}{\partial \xi} - \frac{\partial \psi}{\partial \xi}\frac{\partial \phi}{\partial \theta} + \frac{1}{\sqrt{Gr}Pr}\frac{\partial^2 \phi}{\partial \xi^2} = 0. \tag{24}$$

We first rescale these equations for large Gr using

$$\xi^* = Gr^{1/4}\xi, \quad \phi^* = Gr^{1/4}\phi, \quad \psi^* = Gr^{1/4}\psi, \quad \zeta^* = \frac{\zeta}{Gr^{1/4}}.$$

The factor of $Gr^{1/4}$ follows from the analytical solution given by (19) and is also suggested in [28]. Also note that there is no scaling in θ. This transforms Eqs. (22)–(24) to the following

$$\frac{\partial^2 \psi^*}{\partial \xi^{*2}} = M_0^2 \zeta^*, \tag{25}$$

$$\frac{\partial \psi^*}{\partial \theta}\frac{\partial \zeta^*}{\partial \xi^*} - \frac{\partial \psi^*}{\partial \xi^*}\frac{\partial \zeta^*}{\partial \theta} + \frac{\partial^2 \zeta^*}{\partial \xi^{*2}} + \frac{A_0}{Gr^{1/4}}\frac{\partial \phi^*}{\partial \xi^*} = 0, \tag{26}$$

$$\frac{\partial \psi^*}{\partial \theta}\frac{\partial \phi^*}{\partial \xi^*} - \frac{\partial \psi^*}{\partial \xi^*}\frac{\partial \phi^*}{\partial \theta} + \frac{1}{Pr}\frac{\partial^2 \phi^*}{\partial \xi^{*2}} = 0. \tag{27}$$

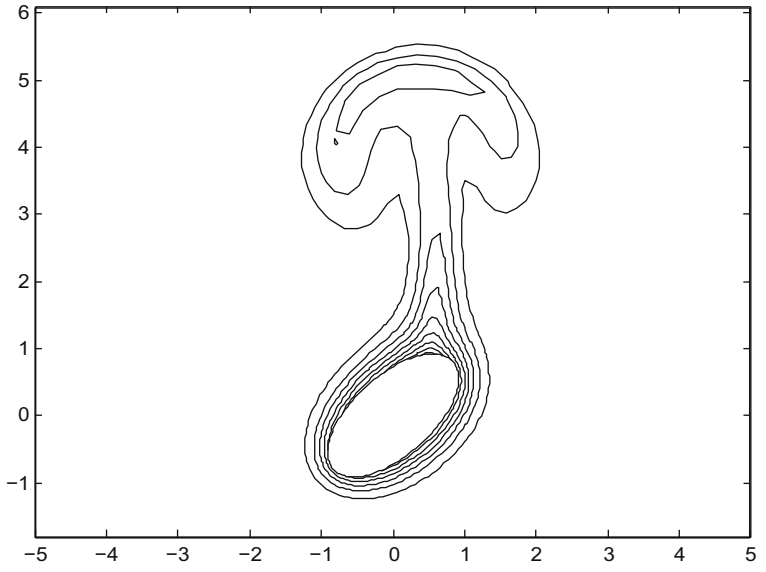

Fig. 10. Isotherm plot at $t = 20$ for the case $Gr = 10^4, Pr = 0.7, r = 0.5$ and $\eta = 45^\circ$.

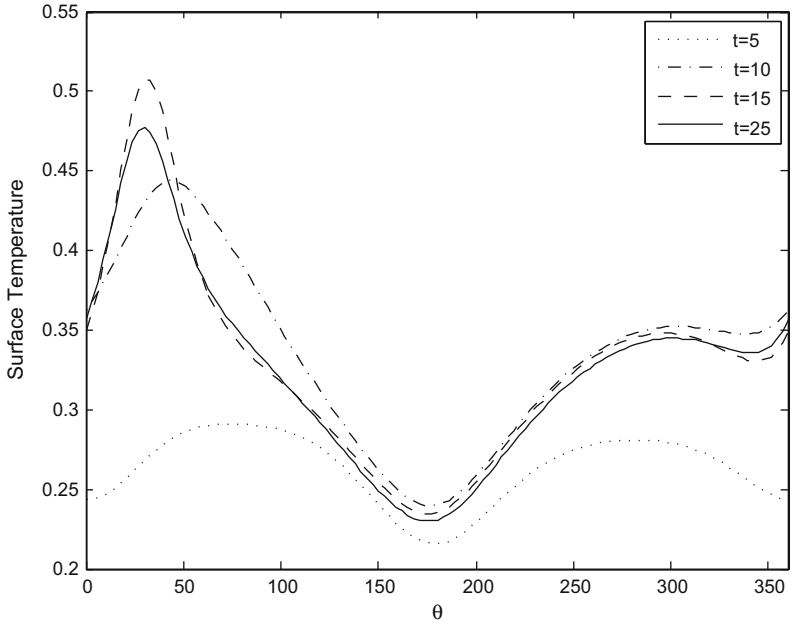

Fig. 11. Surface temperature distributions at various times for the case $Gr = 10^4, Pr = 0.7, r = 0.5$ and $\eta = 45^\circ$.

At this point one may be tempted to discard the buoyancy term in Eq. (26) owing to the factor of $Gr^{-1/4}$. However, this term must be retained since buoyancy is the driving force and omitting it will lead to a contradiction in the analysis. We next apply similar scalings to Eqs. (25)–(27) in terms of Pr:

$$\xi^{**} = Pr^{2/5}\xi^*, \quad \phi^{**} = Pr^{2/5}\phi^*, \quad \psi^{**} = Pr^{3/5}\psi^*, \quad \zeta^{**} = \frac{\zeta^*}{Pr^{1/5}},$$

for the case $Pr \ll 1$, while

$$\xi^{**} = Pr^{1/5}\xi^*, \quad \phi^{**} = Pr^{1/5}\phi^*, \quad \psi^{**} = Pr^{4/5}\psi^*, \quad \zeta^{**} = Pr^{2/5}\zeta^*,$$

for the case $Pr \gg 1$, to obtain the relationships

$$\overline{\phi}_s \propto (Pr)^{-2/5}(Gr)^{-1/4},$$

Table 1
Comparison of $\overline{\phi}_s$ values between the experiments in [20] and our numerical simulations for the case with $Pr = 0.7, r = 0.556$ and $\eta = 90^\circ$.

Heat flux [W/m^2] Q	Grashof number Gr	Experimental $\overline{\phi}_s$	Numerical $\overline{\phi}_s$	Relative error %
54	6.7×10^5	0.18	0.15	17
356	4.4×10^6	0.12	0.10	17
410	5.1×10^6	0.14	0.11	21
600	7.5×10^6	0.12	0.093	23
1200	1.5×10^7	0.11	0.080	27
1620	2.0×10^7	0.090	0.067	26

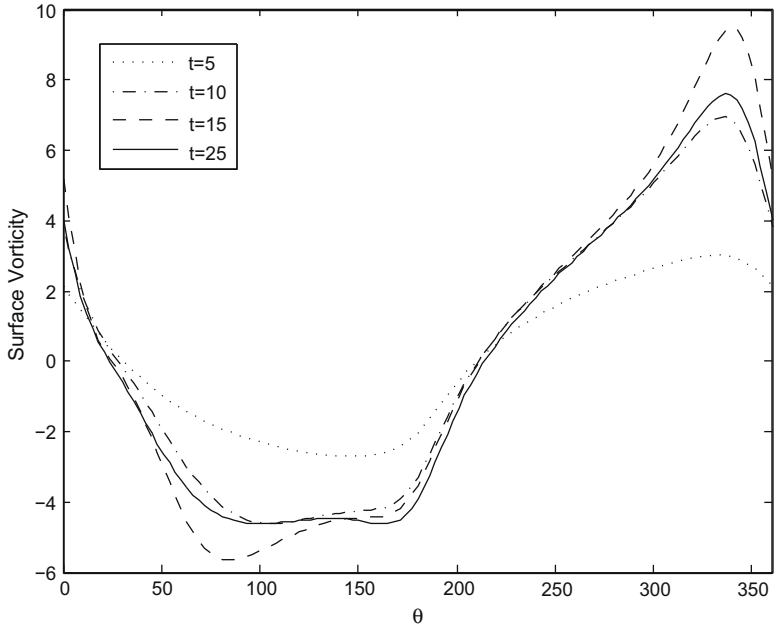

Fig. 12. Surface vorticity distributions at various times for the case $Gr = 10^4, Pr = 0.7, r = 0.5$ and $\eta = 45^\circ$.

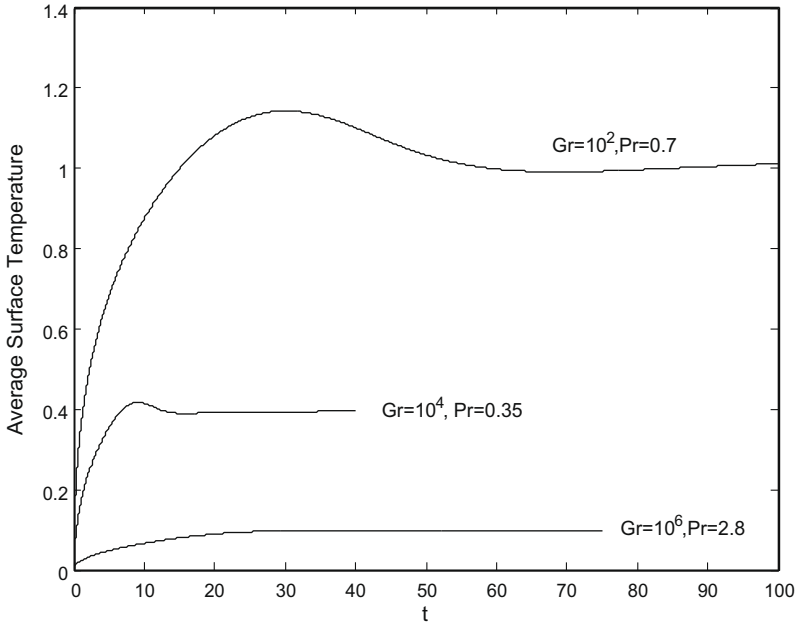

Fig. 13. The time variation of the average surface temperature for various Gr and Pr with $r = 0.5$ and $\eta = 45^\circ$.

for $Gr \gg 1$, $Pr \ll 1$ and

$$\overline{\phi}_s \propto (Pr)^{-1/5}(Gr)^{-1/4},$$

for $Gr \gg 1$, $Pr \gg 1$. Key points worth mentioning in order to arrive at these results are twofold. First, the temperature gradient $\partial\phi^*/\partial\xi^*$ in Eqs. (26) and (27) must be O(1) because of the constant heat flux condition (4). Second, Eq. (26) represents a three-way balance between inertia, viscosity and buoyancy and for the limiting case $Gr \gg 1, Pr \gg 1$ the balance will be between buoyancy and viscosity whereas for the other limiting case $Gr \gg 1, Pr \ll 1$ the balance will be between buoyancy and inertia. Because of numerical difficulties in obtaining solutions for large and small Pr, we were not able to confirm these predictions. However, for $Pr \sim O(1)$ in the range $0.35 \leqslant Pr \leqslant 2.8$ and for $10^2 \leqslant Gr \leqslant 10^6$ our simulations suggest that the following empirical relationship

$$\overline{\phi}_s \approx \frac{3}{(PrGr)^{1/4}},$$

holds reasonably well for an ellipse having $r = 0.5$ inclined at $\eta = 45^\circ$. Fig. 13 illustrates some of these time variations of the average surface temperature for selected values of Gr and Pr.

6. Summary

This paper discussed the unsteady problem of free convection from an inclined elliptic cylinder emitting a constant surface heat flux into an otherwise quiescent viscous incompressible fluid. Some underlying assumptions made in this study include two-dimensionality of the flow, the validity of the Boussinesq approximation, the neglect of viscous dissipation, and that the flow remains laminar. This problem was investigated for the large Grashof number regime both numerically and analytically.

The key contributions offered by this work include a mathematical formulation which is well-suited to address the initial development of the flow and heat transfer process, an analytical solution procedure which is successful in capturing the early stages of the problem, and a robust numerical solution procedure tailored for impulsively generated flows over a wide range of Gr. Direct comparisons with experiments for large-time numerical simulations as well as extensive comparisons between the numerical and analytical solutions for small times were conducted and the agreement in all cases was found to be satisfactory. The large-time simulations have suggested that the average surface temperature appears to approach a steady-state value which can be represented approximately by the relationship

$$\overline{\phi}_s \approx \frac{3}{(PrGr)^{1/4}},$$

over the intervals $10^2 \leqslant Gr \leqslant 10^6$ and $0.35 \leqslant Pr \leqslant 2.8$ for $r = 0.5$ and $\eta = 45^\circ$. Further, scaling arguments suggest that for $Gr \gg 1, Pr \ll 1$

$$\overline{\phi}_s \propto (Pr)^{-2/5}(Gr)^{-1/4},$$

while for $Gr \gg 1$, $Pr \gg 1$

$$\overline{\phi}_s \propto (Pr)^{-1/5}(Gr)^{-1/4}.$$

While the analytical solution derived in this study may have limited usefulness, it is still important given that the exact solution is still unknown. One important application it may serve is to furnish an initial condition which can be used in conjunction with a numerical solution procedure. As mentioned earlier, numerical solutions involving impulsive startups require very small time steps to get past the initial singularity. Using an analytical solution as an initial condition at a small time beyond the singularity at $t = 0$ can assist a numerical procedure and make it run more efficiently.

Acknowledgement

Financial support for this research was provided by the Natural Sciences and Engineering Research Council of Canada.

Appendix A. Asymptotic solution

The details surrounding the double expansion procedure outlined in Section 3 are presented below. The leading-order term for the temperature, ϕ_0, satisfies the equation

$$\frac{1}{PrM_0^2}\frac{\partial^2\phi_0}{\partial z^2}+2z\frac{\partial\phi_0}{\partial z}=4t\frac{\partial\phi_0}{\partial t}. \tag{A1}$$

If we introduce a new coordinate $w=\sqrt{Pr}M_0z$ then the equation simplifies further to

$$\frac{\partial^2\phi_0}{\partial w^2}+2w\frac{\partial\phi_0}{\partial w}=4t\frac{\partial\phi_0}{\partial t}.$$

The most direct way to solve the above is by separation of variables where we set $\phi_0(w,t)=X(w)Y(t)$. A straight-forward calculation reveals that

$$Y(t)\sim t^{\mu/4},\quad X(w)\sim \mathrm{e}^{-w^2/2}f(w),$$

where μ is the separation constant and the function $f(w)$ satisfies

$$\frac{d^2f}{dw^2}-(1+\mu+w^2)f=0,$$

whose solutions involve the Parabolic Cylinder Functions. By resorting to properties of the Parabolic Cylinder Functions [33] it follows that the only solution satisfying the conditions

$$\frac{\partial\phi_0}{\partial w}=0\quad\text{on } w=0\qquad\text{and}\qquad\phi_0\to0\quad\text{as } w\to\infty,$$

is the trivial solution $\phi_0=0$.

The first non-zero term in the temperature expansion corresponds to ϕ_1 and satisfies the equation

$$\frac{1}{PrM_0^2}\frac{\partial^2\phi_1}{\partial z^2}+2z\frac{\partial\phi_1}{\partial z}-2\phi_1=4t\frac{\partial\phi_1}{\partial t}. \tag{A2}$$

Separation of variables is not helpful in solving (A2) since the initial condition is not known for $\phi_n, n\neq0$. Instead, we carry out a second expansion in t in order to make analytical progress. In terms of the coordinate w the equations that result are effectively differential equations and are given by

$$\frac{d^2\phi_{10}}{dw^2}+2w\frac{d\phi_{10}}{dw}-2\phi_{10}=0, \tag{A3}$$

$$\frac{d^2\phi_{1n}}{dw^2}+2w\frac{d\phi_{1n}}{dw}-(2+4n)\phi_{1n}=0, \tag{A4}$$

for $n=1,2,3,\ldots$ These equations must be solved subject to the boundary conditions

$$\frac{d\phi_{10}}{dw}=-\frac{1}{\sqrt{Pr}},\quad\frac{d\phi_{1n}}{dw}=0\quad\text{on } w=0,$$

which follow from the flux condition (12), and the far-field conditions

$$\phi_{10},\phi_{1n}\to0\quad\text{as } w\to\infty.$$

Solving (A3) and (A4) yields

$$\phi_{10}(w)=\frac{1}{\sqrt{\pi}\sqrt{Pr}}\,\mathrm{e}^{-w^2}-\frac{w}{\sqrt{Pr}}\mathrm{erfc}(w)\qquad\text{and}\qquad\phi_{1n}(w)=0\quad\text{for } n=1,2,3,\ldots$$

Thus, we arrive at $\phi_1(t,w)=\phi_{10}(w)$ and the first-order approximation to the temperature becomes $\phi\sim\lambda\phi_1$ which is in complete agreement with the solution given by (19).

Continuing this procedure we have found that

$$\phi_{20}(w,\theta)=\frac{\sinh(2\xi_0)}{8PrM_0^3}\left[\mathrm{erf}(w)\left(w^2+\frac{1}{2}\right)-\frac{w\mathrm{e}^{-w^2}}{\sqrt{\pi}}\right]\qquad\text{and}\qquad\phi_{2n}(w,\theta)=0\quad\text{for } n=1,3,4,\ldots,$$

while $\phi_{22}(w,\theta)$ was not determined. Hence, we can conclude that $\phi_2(t,w,\theta)=\phi_{20}+O(t^2)$. As expected, the procedure gets more and more complicated as more terms are sought and higher-order terms must be determined numerically. Given that a numerical solution procedure for solving the full system of Eqs. (1)–(3) and (9)–(11) is the focus of Section 4, there is no benefit in pursuing higher-order terms. Summarizing, the approximate analytical solution for the temperature is given by

$$\phi(t,w,\theta)=\lambda\phi_{10}+\lambda^2\phi_{20}+O(\lambda^2t^2+\lambda^3).$$

We next solve for the leading-order term in the vorticity expansion. If we introduce another coordinate $s=M_0z$, then the leading-order term, ζ_0, satisfies the equation

$$\frac{\partial^2\zeta_0}{\partial s^2}+2s\frac{\partial\zeta_0}{\partial s}=4t\frac{\partial\zeta_0}{\partial t}-4tA_0\frac{\partial\phi_1}{\partial s}. \tag{A5}$$

Further expanding in t, the problem reduces to solving the following differential equations

$$\frac{d^2\zeta_{00}}{ds^2}+2s\frac{d\zeta_{00}}{ds}=0,$$

$$\frac{d^2\zeta_{01}}{ds^2}+2s\frac{d\zeta_{01}}{ds}-4\zeta_{01}=-4A_0\frac{d\phi_{10}}{ds},$$

$$\frac{d^2\zeta_{0n}}{ds^2}+2s\frac{d\zeta_{0n}}{ds}-4n\zeta_{0n}=0,$$

for $n=2,3,4,\ldots$, subject to the far-field conditions

$$\zeta_{0n}\to0\quad\text{as}\quad s\to\infty\quad\text{for } n=0,1,2,\ldots,$$

along with the integral conditions

$$\int_0^\infty\int_0^{2\pi}M_0\zeta_{0n}\sin(n'\theta)d\theta ds=0,\quad\int_0^\infty\int_0^{2\pi}M_0\zeta_{0n}\cos(n'\theta)d\theta ds=0,$$

for $n,n'=0,1,2,\ldots$ It immediately follows from the initial condition (15) that $\zeta_{00}(s,\theta)=0$ while the general solution for ζ_{01} for $Pr=1$ becomes

$$\zeta_{01}(s,\theta)=D_1(\theta)\left[s\mathrm{e}^{-s^2}-\sqrt{\pi}\left(s^2+\frac{1}{2}\right)\mathrm{erfc}(s)\right]+A_0(\theta)\left[\left(s^2-\frac{1}{2}\right)\mathrm{erfc}(s)-\frac{s\,\mathrm{e}^{-s^2}}{\sqrt{\pi}}\right],$$

whereas for $Pr\neq1$ we obtain

$$\zeta_{01}(s,\theta)=D_2(\theta)\left[s\mathrm{e}^{-s^2}-\sqrt{\pi}\left(s^2+\frac{1}{2}\right)\mathrm{erfc}(s)\right]-2A_0(\theta)\left[\frac{1}{(1-Pr)}\left(s^2+\frac{1}{2}\right)\mathrm{erfc}(\sqrt{Pr}s)\right]+2A_0(\theta)\left[s^2\mathrm{erfc}(\sqrt{Pr}s)+\frac{\sqrt{Pr}}{\sqrt{\pi}(1-Pr)}s\mathrm{e}^{-Prs^2}\right].$$

In the above $D_1(\theta)$ and $D_2(\theta)$ represent Fourier series that emerge from enforcing the integral conditions above, and were computed numerically. Further, we have shown that $\zeta_{0n}(s,\theta)=0$ for $n=2,3,4,\ldots$, and that $\zeta_{10}(s,\theta)=0$. Summarizing, we obtain $\zeta_0(t,s,\theta)=t\zeta_{01}$ and the approximate analytical solution for the vorticity is

$$\zeta(t,s,\theta)=t\zeta_{01}+O(t^2+\lambda t).$$

Lastly, we solve for the streamfunction. Due to the no-slip and impermeable boundary conditions on the surface given by (12), it is easily shown that the first two terms in the series for the streamfunction are simply $\psi_0=\psi_1=0$. The non-zero leading-order problem then corresponds to solving

$$\frac{\partial^2\psi_2}{\partial z^2}=M_0^2t\zeta_0. \tag{A6}$$

Making use of the double expansion and $s = M_0 z$, the problem reduces to solving the following differential equations

$$\frac{d^2\psi_{21}}{ds^2} = \zeta_{01} \quad \text{and} \quad \frac{d^2\psi_{2n}}{ds^2} = 0 \quad \text{for } n = 0, 2, 3, \ldots$$

Solving these equations subject to the no-slip and impermeable conditions, we find that $\psi_{2n}(s,\theta) = 0$ for $n = 0, 2, 3, \ldots$, while for $Pr = 1$

$$\begin{aligned}\psi_{21}(s,\theta) = {} & \frac{\sqrt{\pi}}{16}\left(D_1(\theta) + \frac{3A_0(\theta)}{\sqrt{\pi}}\right)\mathrm{erf}(s) \\ & - \frac{\sqrt{\pi}}{12}\left[D_1(\theta)\mathrm{erfc}(s) - \frac{A_0(\theta)}{\sqrt{\pi}}\mathrm{erfc}(s)\right]s^4 \\ & + \frac{1}{12}\left(D_1(\theta) - \frac{A_0(\theta)}{\sqrt{\pi}}\right)s^3 e^{-s^2} + \frac{1}{24}\left(5D_1(\theta) + \frac{7A_0(\theta)}{\sqrt{\pi}}\right)s e^{-s^2} \\ & - \frac{\sqrt{\pi}}{4}\left(D_1(\theta) + \frac{A_0(\theta)}{\sqrt{\pi}}\right)s^2\mathrm{erfc}(s) - \frac{1}{3}\left(D_1(\theta) + \frac{2A_0(\theta)}{\sqrt{\pi}}\right)s,\end{aligned}$$

and for $Pr \neq 1$

$$\begin{aligned}\psi_{21}(s,\theta) = {} & \frac{1}{16}D_2(\theta)\sqrt{\pi}\,\mathrm{erf}(s) + \left(\frac{3A_0(\theta)}{8(1-Pr)} + \frac{A_0(\theta)}{4Pr(1-Pr)}\right)\mathrm{erf}(\sqrt{Pr}s) \\ & - \left(\frac{D_2(\theta)\sqrt{\pi}}{12} + \frac{PrA_0(\theta)}{6(1-Pr)}\right)s^4 + \frac{A_0(\theta)}{6(1-Pr)}s^4\mathrm{erf}(\sqrt{Pr}s) \\ & + \frac{D_2(\theta)\sqrt{\pi}}{12}s^4\mathrm{erf}(s) + \frac{D_2(\theta)}{12}s^3 e^{-s^2} + \frac{\sqrt{Pr}A_0(\theta)}{6(1-Pr)\sqrt{\pi}}s^3 e^{-Prs^2} \\ & + \frac{5D_2(\theta)}{24}s e^{-s^2} - \left(\frac{D_2(\theta)\sqrt{\pi}}{2} + \frac{A_0(\theta)}{(1-Pr)}\right)\frac{s^2}{2} \\ & + \frac{D_2(\theta)\sqrt{\pi}}{4}s^2\mathrm{erf}(s) + \frac{A_0(\theta)}{2(1-Pr)}s^2\mathrm{erf}(\sqrt{Pr}s) \\ & + \left(\frac{A_0(\theta)}{2(1-Pr)\sqrt{Pr\pi}} - \frac{\sqrt{Pr}A_0(\theta)}{12(1-Pr)\sqrt{Pr\pi}}\right)s e^{-Prs^2} \\ & - \left(\frac{D_2(\theta)}{3} + \frac{2\sqrt{Pr}A_0(\theta)}{3(1-Pr)\sqrt{\pi}}\right)s.\end{aligned}$$

Thus, we obtain $\psi_2(t,s,\theta) = t\psi_{21}$ and note that ψ_{21} diverges as $s \to \infty$. This is because we chose to apply the surface conditions instead of the far-field condition when solving for ψ_{21}. Finally, the approximate analytical solution for the streamfunction becomes

$$\psi(t,s,\theta) = \lambda^2 t\psi_{21} + O(\lambda^3).$$

As a final note, the expansion procedure has been continued further numerically and more terms are reported in [34].

References

[1] A.P. Bassom, P.J. Blennerhassett, Impulsively generated convection in a semi-infinite fluid layer above a heated flat plate, Q. J. Mech. Appl. Math. 55 (2002) 573–595.

[2] F.J. Suriano, K.T. Yang, Laminar free convection about vertical and horizontal plates at small and moderate Grashof numbers, Int. J. Heat Mass Transfer 11 (1968) 473–492.

[3] S.W. Churchill, H.H. Chu, Correlating equations for laminar and turbulent free convection from a vertical plate, Int. J. Heat Mass Transfer 18 (1975) 1323–1329.

[4] R.J. Goldstein, D.G. Briggs, Transient free convection about vertical plates and circular cylinders, ASME J. Heat Transfer 86C (1964) 490–500.

[5] N.E. Hardwick, E.K. Levy, Study of laminar free convection wake above an isothermal vertical plate, ASME J. Heat Transfer 95 (1973) 289–294.

[6] E.M. Sparrow, S.V. Patanker, R.M. Abdel-Wahed, Development of wall and free plumes above a heated vertical plate, ASME J. Heat Transfer 100 (1978) 184–190.

[7] R. Chouikh, A. Guizani, M. Maalej, A. Gelghith, Numerical study of the laminar natural convection flow around horizontal isothermal cylinder, Renewable Energy 13 (1998) 77–88.

[8] T. Saitoh, T. Sajiki, K. Maruhara, Bench mark solutions to natural convection heat transfer problem around a horizontal circular cylinder, Int. J. Heat Mass Transfer 36 (1993) 1251–1259.

[9] M.A. Atmane, V.S.S. Chan, D.B. Murray, Natural convection around a horizontal heated cylinder: the effects of vertical confinement, Int. J. Heat Mass Transfer 46 (2003) 3661–3672.

[10] H.M. Badr, Heat transfer in transient buoyancy driven flow adjacent to a horizontal rod, Int. J. Heat Mass Transfer 30 (1987) 1997–2012.

[11] L. Elliot, Free convection on a two-dimensional or axisymmetric body, Q. J. Mech. Appl. Math. 23 (1970) 153–162.

[12] B. Farouck, S.I. Guceri, Natural convection from a horizontal cylinder – laminar regime, ASME J. Heat Transfer 103 (1981) 522–527.

[13] T.H. Kuehn, R.J. Goldstein, Numerical solution to the Navier–Stokes equations for laminar natural convection about a horizontal isothermal circular cylinder, Int. J. Heat Mass Transfer 23 (1980) 971–979.

[14] J.H. Merkin, Free convection on an isothermal horizontal cylinder, ASME Paper No. 76-HT-16, 1976.

[15] L. Pera, B. Gebhart, Experimental observations of wake formation over cylindrical surfaces in natural convection flows, Int. J. Heat Mass Transfer 15 (1972) 175–177.

[16] H.M. Badr, K. Shamsher, Free convection from an elliptic cylinder with major axis vertical, Int. J. Heat Mass Transfer 36 (1993) 3593–3602.

[17] F.M. Mahfouz, S. Kocabiyik, Transient numerical simulation of buoyancy driven flow adjacent to an elliptic tube, Int. J. Heat Fluid Flow 24 (2003) 864–873.

[18] H.M. Badr, Laminar natural convection from an elliptic tube with different orientations, J. Heat Transfer 119 (1997) 709–718.

[19] S.Y. Huang, F. Mayinger, Heat transfer with natural convection around elliptic tubes, Warme-Und Stoffubertragung 18 (1984) 175–183.

[20] A.O. Elsayed, E.Z. Ibrahim, S.A. Elsayed, Free convection from a constant heat flux elliptic tube, Energy Convers. Manage. 44 (2003) 2445–2453.

[21] F.N. Lin, B.T. Chao, Laminar free convection over two-dimensional and axisymmetric bodies of arbitrary contour, ASME J. Heat Transfer 96 (1974) 435–442.

[22] J.H. Merkin, Free convection boundary layers on cylinders of elliptic cross section, ASME J. Heat Transfer 99 (1977) 453–457.

[23] G.D. Raithby, K.G. Hollands, Laminar and turbulent free convection from elliptic cylinders with a vertical plate and horizontal circular cylinder as special cases, ASME J. Heat Transfer 98 (1976) 72–80.

[24] G.P. Fieg, W. Roetzel, Calculation of laminar film condensation in/on inclined elliptical tubes, Int. J. Heat Mass Transfer 37 (1994) 619–624.

[25] S.B. Memory, V.H. Adams, P.J. Marto, Free and forced convection laminar film condensation on horizontal elliptical tubes, Int. J. Heat Mass Transfer 40 (1997) 3395–3406.

[26] S.J.D. D'Alessio, L.A. Finlay, J.P. Pascal, Free convection from elliptic cylinders at small Grashof numbers, Int. J. Heat Mass Transfer 51 (2008) 1379–1392.

[27] A. Liñán, V.N. Kurdyumov, Laminar free convection induced by a line heat source and heat transfer from wires at small Grashof numbers, J. Fluid Mech. 362 (1998) 199–227.

[28] L.G. Leal, Laminar Flow and Convection Transport Processes: Scaling Principles and Asymptotic Analysis, Butterworth-Heinemann, Boston, 1992.

[29] C.-S. Yih, Laminar free convection due to a line source of heat, Trans. Am. Geophys. Union 33 (1952) 669–672.

[30] A.N. Staniforth, Studies of symmetrical and asymmetrical viscous flows past impulsively started cylinders, Ph.D. thesis, University of Western Ontario, London, Ontario, 1973.

[31] S.C.R. Dennis, L. Quartapelle, Some uses of Green's theorem in solving the Navier–Stokes equations, Int. J. Numer. Meth. Fluids 9 (1989) 871–890.

[32] M.L. Williams, Analytic study of unsteady free convection from an inclined elliptic cylinder, M.Math. thesis, University of Waterloo, Waterloo, Ontario, 2004.

[33] H. Bateman, A. Erdelyi, Higher Transcendental Functions, vol. 2, McGraw-Hill, New York, 1953.

[34] R.N. Perera, Unsteady free convection from elliptic tubes at large Grashof numbers, M.Math. thesis, University of Waterloo, Waterloo, Ontario, 2008.